

Numerical Study of Differential Equations Via Cubic Hermite Collocation Technique

Happy Kumar

Assistant Professor in Mathematics, Guru Nanak College, Budhlada (Mansa), Punjab, India

Email: happygarg85@gmail.com

Abstract: The cubic Hermite collocation method (CHCM) is a numerical technique for solving differential equations using Cubic Hermite interpolation. Cubic Hermite interpolation is a way of constructing a polynomial that matches not only the function values, but also the derivatives at some given points. The accuracy, efficiently, simplicity and reliability of CHCM performs are demonstrated through some numerical examples. The analysis of convergence of the method is briefly discussed and the fourth order is shown. The Numerical results have been presented in tabular and graphical forms.

Keywords: CHCM, graphical forms, Numerical

1 Introduction

The numerical analysis literature contains vast on the solution of differential equations which arise in the mathematical modeling via convection diffusion process (Grahs (1974), Al-Jabari 1994, Potucek 1997). Orthogonal collocation method (Maleknejad et al. 2006, Shen & Lin 2006 and Soliman & Alhumaizi (2004).) is well established as robust techniques for solving differential equations. Lagrange interpolating approximations to boundary element equations are not new either. Initially introduced by Carey & Finlayson 1975 and developed further by a number of authors (Arora et. al. 2006, Islam et al. 2010, Kim & Shin 2002) they have not been widely adopted due to the additional degrees of freedom introduced by the derivatives. It increases the number of collocation equation at node points. To overcome this problem by technique of Cubic Hermite interpolating has been used in association with orthogonal collocation.

In Hermite collocation method, the approximating function is discretized in terms of cubic Hermite polynomial and then orthogonal collocation is applied. Due to continuity property of cubic Hermite polynomials there is no need add the additional property that approximating function and its first derivative should be continuous at nodes points.

In the present study, cubic Hermite collocation method is use for solving differential equations.

2 Hermite collocation method

In present study, cubic Hermite interpolating polynomials as discussed by (Dyksen & Lynch 2000 and Brill 2002) have been followed to solve the boundary value problems numerically and are defined as:

$$P_j(\xi) = \begin{cases} 3 \left(\frac{\xi_{j+1}-\xi}{\xi_{j+1}-\xi_j} \right)^2 - 2 \left(\frac{\xi_{j+1}-\xi}{\xi_{j+1}-\xi_j} \right)^3, & \xi_j \leq \xi \leq \xi_{j+1} \\ 3 \left(\frac{\xi-\xi_{j-1}}{\xi_j-\xi_{j-1}} \right)^2 - 2 \left(\frac{\xi-\xi_{j-1}}{\xi_j-\xi_{j-1}} \right)^3, & \xi_{j-1} \leq \xi \leq \xi_j \\ 0, & \text{elsewhere} \end{cases} \quad (1)$$

$$\bar{P}_j(\xi) = \begin{cases} \frac{(\xi_{j+1}-\xi)^2}{\xi_{j+1}-\xi_j} - \frac{(\xi_{j+1}-\xi)^3}{(\xi_{j+1}-\xi_j)^2}, & \xi_j \leq \xi \leq \xi_{j+1} \\ -\frac{(\xi-\xi_{j-1})^2}{\xi_j-\xi_{j-1}} + \frac{(\xi-\xi_{j-1})^3}{(\xi_j-\xi_{j-1})^2}, & \xi_{j-1} \leq \xi \leq \xi_j \\ 0, & \text{elsewhere} \end{cases} \quad (2)$$

These piecewise cubics are designed such that $P_j(\xi_i) = \delta_{ji}, P_j'(\xi_i) = 0, \bar{P}_j(\xi_i) = 0, \bar{P}_j'(\xi_i) = \delta_{ji}$.

By rearranging the terms in eq. (1) and eq. (2), Hermite interpolating polynomials can be rewritten as:

$$H_i(\xi) = \begin{cases} 3 \left(\frac{\xi_{i+1}-\xi}{\xi_{i+1}-\xi_i} \right)^2 - 2 \left(\frac{\xi_{i+1}-\xi}{\xi_{i+1}-\xi_i} \right)^3, & \xi_i \leq \xi \leq \xi_{i+1} \\ 3 \left(\frac{\xi-\xi_{i-1}}{\xi_i-\xi_{i-1}} \right)^2 - 2 \left(\frac{\xi-\xi_{i-1}}{\xi_i-\xi_{i-1}} \right)^3, & \xi_{i-1} \leq \xi \leq \xi_i \\ \frac{(\xi_{i+1}-\xi)^2}{\xi_{i+1}-\xi_i} - \frac{(\xi_{i+1}-\xi)^3}{(\xi_{i+1}-\xi_i)^2}, & \xi_i \leq \xi \leq \xi_{i+1} \\ -\frac{(\xi-\xi_{i-1})^2}{\xi_i-\xi_{i-1}} + \frac{(\xi-\xi_{i-1})^3}{(\xi_i-\xi_{i-1})^2}, & \xi_{i-1} \leq \xi \leq \xi_i \\ 0, & \text{elsewhere} \end{cases} \quad (3)$$

The first order derivative of cubic Hermite basis is defined as:

$$H_i'(\xi) = \begin{cases} -6 \frac{\xi_{i+1}-\xi}{(\xi_{i+1}-\xi_i)^2} + 6 \frac{(\xi_{i+1}-\xi)^2}{(\xi_{i+1}-\xi_i)^3}, & \xi_i \leq \xi \leq \xi_{i+1} \\ 6 \frac{\xi-\xi_{i-1}}{(\xi_i-\xi_{i-1})^2} - 6 \frac{(\xi-\xi_{i-1})^2}{(\xi_i-\xi_{i-1})^3}, & \xi_{i-1} \leq \xi \leq \xi_i \\ -2 \frac{\xi_{i+1}-\xi}{\xi_{i+1}-\xi_i} + 3 \left(\frac{\xi_{i+1}-\xi}{\xi_{i+1}-\xi_i} \right)^2, & \xi_i \leq \xi \leq \xi_{i+1} \\ -2 \frac{\xi-\xi_{i-1}}{\xi_i-\xi_{i-1}} + 3 \left(\frac{\xi-\xi_{i-1}}{\xi_i-\xi_{i-1}} \right)^2, & \xi_{i-1} \leq \xi \leq \xi_i \\ 0, & \text{elsewhere} \end{cases} \quad (4)$$

The behavior of Hermite cubics $P_0, P_1, \bar{P}_0, \bar{P}_1$ is shown in Figure 1.

3 Collocation Points

In Hermite collocation, the choice of collocation points depends upon the degree of the interpolating polynomial. In present study, cubic Hermite polynomials have been taken as interpolating polynomials, therefore, two collocation points have been taken within each interval $[\zeta_{j-1}, \zeta_j]$ and $[\zeta_j, \zeta_{j+1}]$. To apply orthogonal collocation within each interval $[\zeta_{j-1}, \zeta_j]$ a new variable ζ is introduced in such a way that $\zeta = \frac{\xi-\xi_{j-1}}{h_j}$ where $h_j = \xi_j - \xi_{j-1}$ such that $\zeta = 0$ when $\xi = \xi_{j-1}$ and $\zeta = 1$ when $\xi = \xi_j$. Roots of shifted Legendre polynomial of order two have been calculated as:

$$\zeta_i = \frac{\sqrt{3}+1}{2\sqrt{3}}; \quad i = 1, 2 \quad (5)$$

4 Application of Hermite Collocation Method to Initial Boundary Value Problems

Consider the following initial boundary value problem:

$$y_\tau = \bar{\epsilon} y_{\xi\xi} - \bar{\alpha}(\xi) y_\xi - \bar{\beta}(\xi) y + f(\xi) \quad \forall (\zeta, \tau) \in \Omega \times (0, T) \quad (6)$$

where $y_\tau = \frac{\partial y}{\partial \tau}$, $y_{\xi\xi} = \frac{\partial^2 y}{\partial \xi^2}$, $y_\xi = \frac{\partial y}{\partial \xi}$, and $f(\zeta)$ is a continuous function of ζ . $\bar{\alpha}(\xi)$ and $\bar{\beta}(\xi)$ are continuous functions of ζ such that $\bar{\alpha}(\xi)$ and $\bar{\beta}(\xi)$ are positive bounded functions possessing continuous derivatives for all $\zeta \in \Omega$.

The boundary conditions along the layers are assumed to be of Robinson's type or mixed conditions:

$$y - \bar{\epsilon} y_\xi = 0 \quad \text{at } \zeta = 0, \forall \tau > 0 \quad (7)$$

$$y_\xi = 0 \quad \text{at } \zeta = 1, \forall \tau > 0 \quad (8)$$

$$\text{Initially, it is assumed that } y_0 = y(\zeta, 0) = 1; \forall \zeta \in \Omega \quad (9)$$

The cubic Hermite approximation is defined as:

$$y(\xi, \tau) = \sum_{i=1}^m a_i(\tau) H_i(\xi), \quad \forall \zeta \in [\zeta_{i-1}, \zeta_{i+1}] \quad (10)$$

Where, $a_i(\tau)$'s are the continuous functions of ' τ '. The continuous functions $a_i(\tau)$'s are arranged in such a way in the interval $[\zeta_{i-1}, \zeta_i]$ and $[\zeta_i, \zeta_{i+1}]$ that the problem of double collocation omits out. The behaviour of these polynomials in the interval $[\zeta_{i-1}, \zeta_i]$ and $[\zeta_i, \zeta_{i+1}]$ is shown in Figure 2.

5 Rate of Convergence

Next step of the present study is the determination of rate of convergence of the given numerical technique of Hermite collocation. To determine the rate of convergence, method of (Farrell & Hagarty 1991) has been followed. Define the maximum pointwise error as:

$$E_{\bar{\varepsilon}}^m = \|\bar{y}^m - \bar{y}^{2m}\|_{\infty} \tag{11}$$

where \bar{y}^m is the cubic Hermite approximation of $y(\zeta, \tau_i)$ at the m node points. The additional node points in the spatial direction can be added by selecting the mid points of the node points ζ_i 's in the spatial direction for $1 \leq i \leq m$. The $\bar{\varepsilon}$ -uniform error is defined as:

$$E^m = \max_{\bar{\varepsilon}} E_{\bar{\varepsilon}}^m \tag{12}$$

The rate of convergence is calculated as:

$$p_{\bar{\varepsilon}}^m = \frac{\log(E_{\bar{\varepsilon}}^m) - \log(E_{\bar{\varepsilon}}^{2m})}{\log(2)} \tag{13}$$

The $\bar{\varepsilon}$ -uniform rate of convergence is calculated as:

$$p^m = \frac{\log(E^m) - \log(E^{2m})}{\log(2)} \tag{14}$$

Numerical Examples

Problem 1

Consider linear advection-diffusion equation with mixed boundary conditions and

$$\bar{\alpha}(\xi) = \bar{\beta}(\xi) = 1, f(\xi) = \cos \pi \xi.$$

$$\frac{\partial y}{\partial \tau} = \bar{\varepsilon} \frac{\partial^2 y}{\partial \xi^2} - \frac{\partial y}{\partial \xi} - y + \cos \pi \xi \tag{15}$$

Boundary conditions are given as:

$$y(0, \tau) - \bar{\varepsilon} \frac{\partial y}{\partial \xi} \Big|_{\xi=0} = 0, \quad \forall \tau \in (0, T] \tag{16}$$

$$\frac{\partial y}{\partial \xi} \Big|_{\xi=1} = 0, \quad \forall \tau \in (0, T] \tag{17}$$

Initially, it is assumed that $y(\zeta, 0) = 1, \forall \zeta \in \Omega$. In Figure 4, the behaviour of solution profiles is shown at different time intervals for $\bar{\varepsilon} = 2^{-4}$. In Figure 5, the behaviour of solution profiles is shown for different values of $\bar{\varepsilon}$ for 32 mesh points at $\zeta = 1$. The solution profile for $\bar{\varepsilon} = 0.1$ converge to 1 smoothly as τ increases as compare to the profiles of $\bar{\varepsilon} = 0.01$ and $\bar{\varepsilon} = 0.001$. The smoothness in the profiles for small values of $\bar{\varepsilon}$ can be obtained by increasing the number of mesh points. The 3D behaviour of $y(\zeta, \tau)$ for different values of $\bar{\varepsilon}$ is shown in Figure 6a to 6c.

In Table 1, the $\bar{\varepsilon}$ -uniform rate of convergence is shown. It is observed that the $\bar{\varepsilon}$ -uniform rate of convergence varies from 0.98422 to 0.99567 for 8 to 64 mesh points, respectively.

Problem 2

Consider linear advection-diffusion equation with mixed boundary conditions and

$$\bar{\alpha}(\xi) = \bar{\beta}(\xi) = f(\xi) = 1.$$

$$\frac{\partial y}{\partial \tau} = \bar{\varepsilon} \frac{\partial^2 y}{\partial \xi^2} - \frac{\partial y}{\partial \xi} - y + 1 \tag{18}$$

Initial and boundary conditions remain same as of the Problem 1. In Figure 7, the solution profiles are shown at different time intervals for $\bar{\varepsilon} = 2^{-4}$. In Figure 8, the behaviour of solution profiles is shown for different values of $\bar{\varepsilon}$ at $\zeta = 1$ for 32 mesh points. The graphs are found to be approaching to zero smoothly as time increases. The 3D behaviour of $y(\zeta, \tau)$ for different values of $\bar{\varepsilon}$ is shown in Figure 9a to 9c.

In Table 2, the $\bar{\varepsilon}$ -uniform rate of convergence is shown for Problem 2. It is observed that the $\bar{\varepsilon}$ -uniform rate of convergence is 0.96893 to 0.99589 for 8 to 64 mesh points, respectively.

Problem 3

Consider linear advection-diffusion equation with mixed boundary conditions and

$$\bar{\alpha}(\xi) = (1 + \xi^2), \bar{\beta}(\xi) = 1 \text{ and } f(\xi) = \xi^3.$$

$$\frac{\partial y}{\partial \tau} = \bar{\varepsilon} \frac{\partial^2 y}{\partial \xi^2} - (1 + \xi^2) \frac{\partial y}{\partial \xi} - y + \xi^3 \tag{19}$$

Initial and boundary conditions remain same as of the Problem 1. In Figure 10, the solution profiles are shown at different time intervals for $\bar{\varepsilon} = 2^{-4}$. In Figure 11, the behaviour of solution profiles is shown for different values of $\bar{\varepsilon}$ at $\zeta = 1$ for 64 mesh points. The graphs are found to be approaching to zero as time increases. The 3D behaviour of $y(\zeta, \tau)$ for different values of $\bar{\varepsilon}$ is shown in Figure 12a to 12c. In Table 3, the $\bar{\varepsilon}$ -uniform rate of

convergence is shown. It is observed that the $\bar{\epsilon}$ -uniform rate of convergence is 0.99193 to 1.0031 for 16 to 128 mesh points, respectively.

Problem 4

Consider linear advection-diffusion equation with mixed boundary conditions and

$$\bar{\alpha}(\xi) = \bar{\beta}(\xi) = 1 \text{ and } f(\xi) = 0.$$

$$\frac{\partial y}{\partial \tau} = \bar{\epsilon} \frac{\partial^2 y}{\partial \xi^2} - \frac{\partial y}{\partial \xi} - y \tag{20}$$

Initial and boundary conditions remain same as of the Problem 1. In Figure 13, the behaviour of solution profiles is shown for different values of $\bar{\epsilon}$ for 32 mesh points. The solution profile for $\bar{\epsilon} = 0.1$ converge to 1 smoothly as τ increases as compare to the profiles of $\bar{\epsilon} = 0.01$ and $\bar{\epsilon} = 0.001$. The smoothness in the profiles for small values of $\bar{\epsilon}$ can be obtained by increasing the number of mesh points. The 3D behaviour of $y(\xi, \tau)$ for different values of $\bar{\epsilon}$ is shown in Figure 14a to 14c. In Table 4, the $\bar{\epsilon}$ -uniform rate of convergence is shown. It is observed that the $\bar{\epsilon}$ -uniform rate of convergence is found to be 0.96819 to 0.99567 for 8 to 64 mesh points, respectively.

Problem 5

Consider linear advection-diffusion equation with mixed boundary conditions and

$$\bar{\alpha}(\xi) = 1, \bar{\beta}(\xi) = f(\xi) = 0.$$

$$\frac{\partial y}{\partial \tau} = \bar{\epsilon} \frac{\partial^2 y}{\partial \xi^2} - \frac{\partial y}{\partial \xi} \tag{21}$$

Initial and boundary conditions remain same as of the Problem 1. In Figure 15, the behaviour of solution profiles is shown for different values of $\bar{\epsilon}$ for 32 mesh points. The solution profiles are found to converge to zero smoothly as time increases. The 3D behaviour of $y(\xi, \tau)$ for different values of $\bar{\epsilon}$ is shown in Figure 16a to 16c. In Table 5, the $\bar{\epsilon}$ -uniform rate of convergence is shown. It is observed that the $\bar{\epsilon}$ -uniform rate of convergence is 0.98551 to 0.99559 for 8 to 64 mesh points, respectively.

Conclusion

Cubic Hermite collocation method is tested on various initial Value problems for different range of parameter $\bar{\epsilon}$. The method is shown to be uniformly convergent. From these figures and tables, it is observed that the accuracy of the method is of order (h^4) .

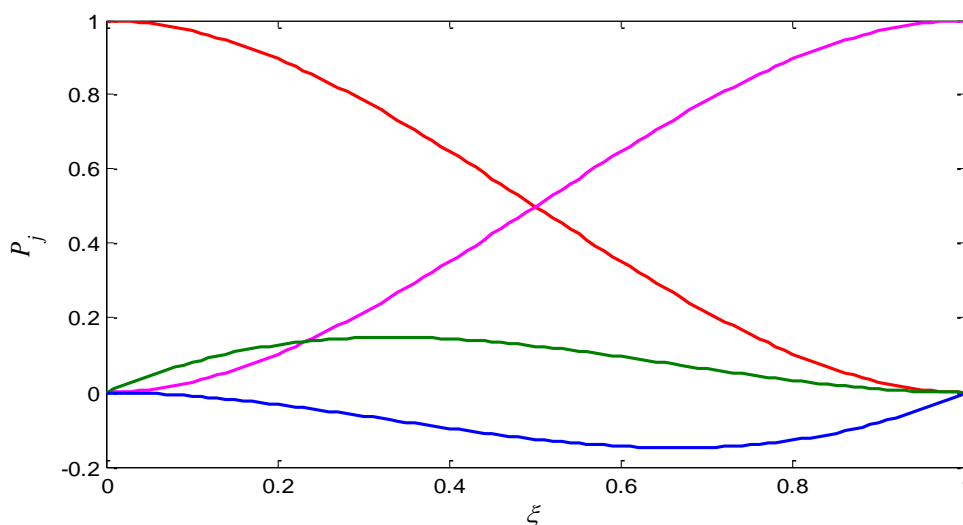


Figure 1: Behavior of Hermite cubics on the interval $[\xi_{i-1}, \xi_{i+1}]$ $P_0(\xi)$ (—), $\bar{P}_0(\xi)$ (◇), $P_1(\xi)$ (□), $\bar{P}_1(\xi)$ (Δ).

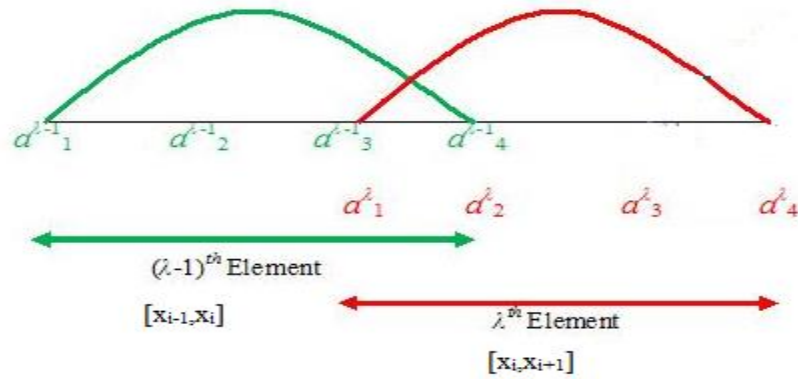


Figure 2: Structure of local Hermite collocation in $[\zeta_{i-1}, \zeta_i]$ and $[\zeta_i, \zeta_{i+1}]$.

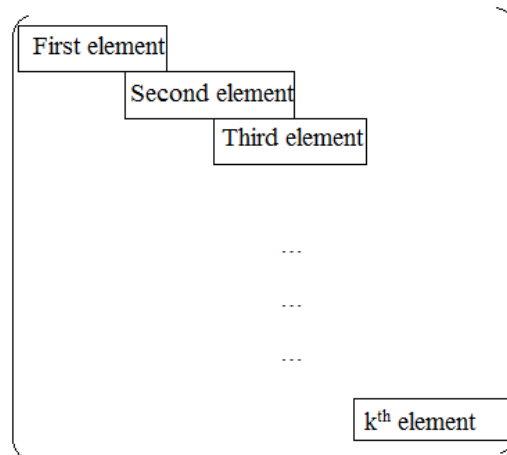


Figure 3: Each block consists of system of linear differential equations defined at j^{th} collocation point in the sub-interval $[\zeta_{i-1}, \zeta_i]$.

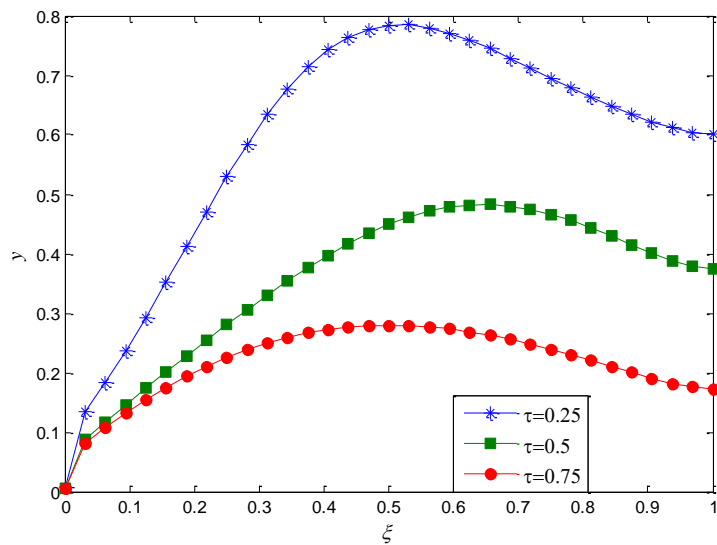


Figure 4: Behavior of $y(\xi, \tau)$ for $\bar{\epsilon} = 2^{-4}$ at different time intervals for Problem 1.

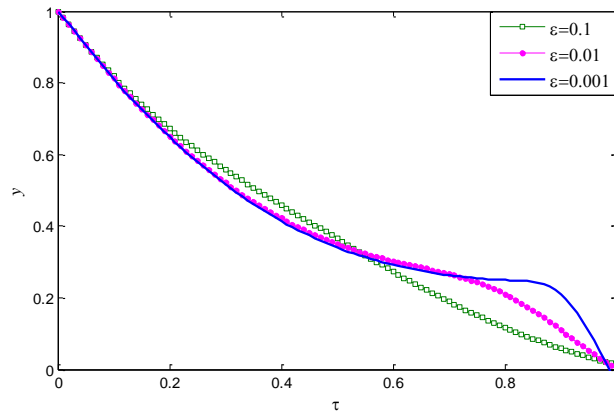


Figure 5: Behavior of $y(\xi, \tau)$ for different values of $\bar{\epsilon}$.

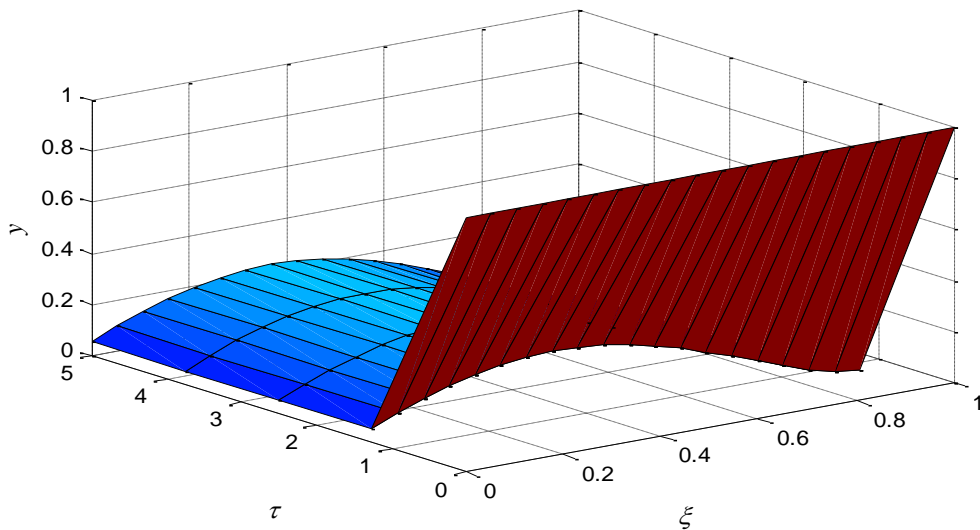


Figure 6a: 3D behaviour of $y(\xi, \tau)$ for $\bar{\epsilon} = 2^{-4}$.

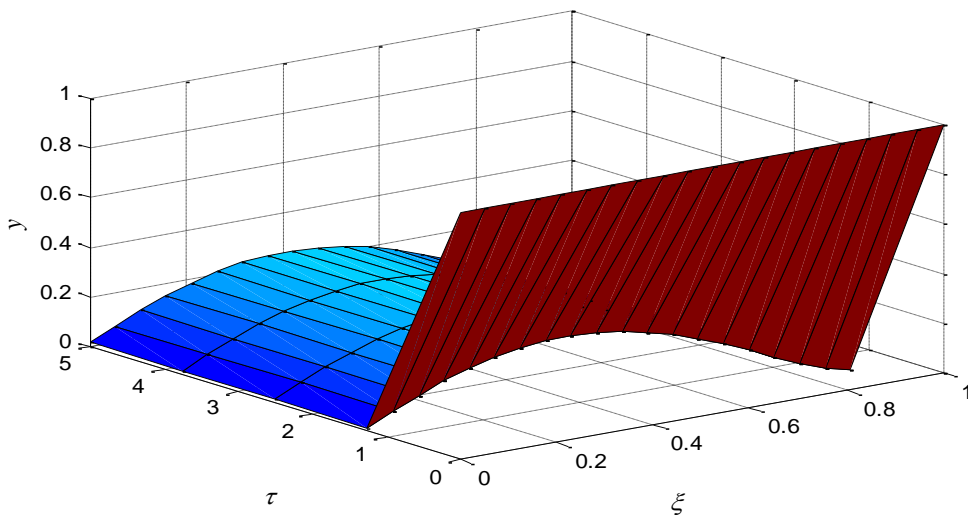


Figure 6b: 3D behaviour of $y(\xi, \tau)$ for $\bar{\epsilon} = 2^{-6}$.

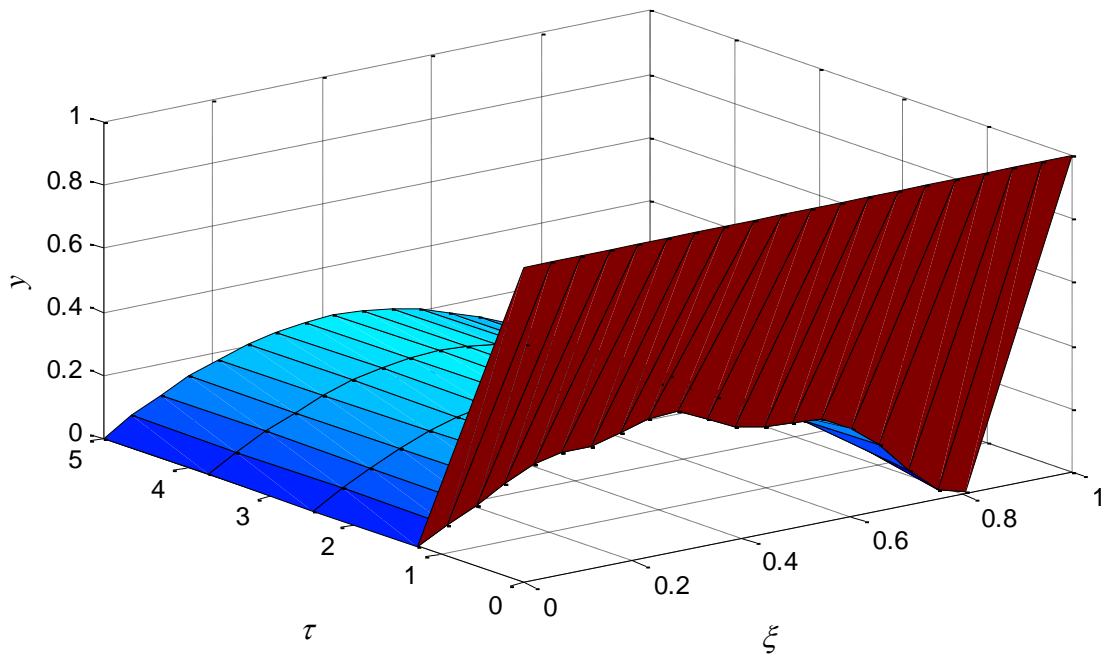


Figure 6c: 3D behaviour of $y(\xi, \tau)$ for $\bar{\varepsilon} = 2^{-10}$.

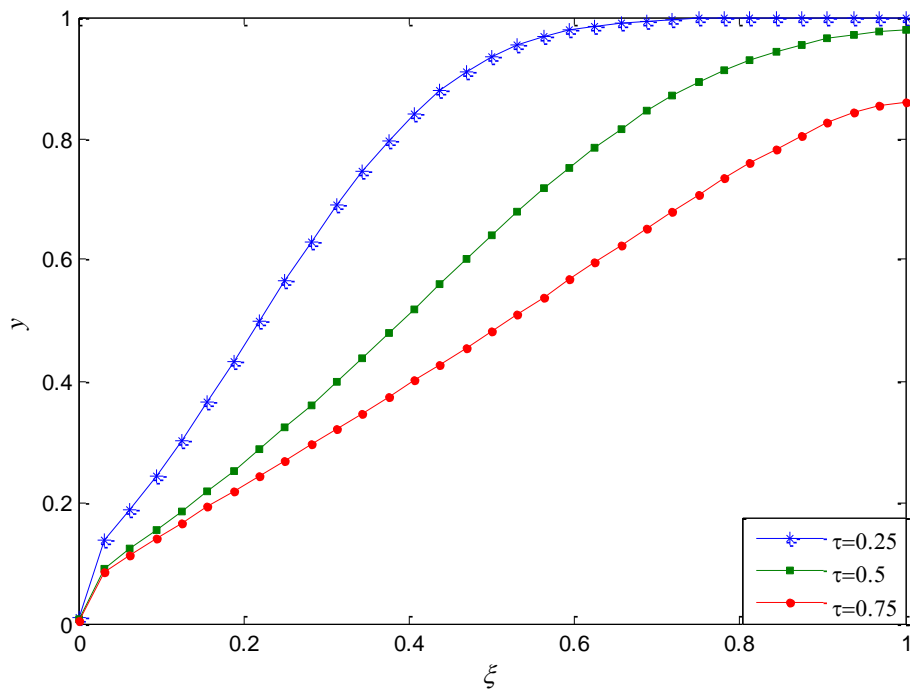


Figure 7: Behavior of $y(\xi, \tau)$ for $\bar{\varepsilon} = 2^{-4}$ at different time intervals for Problem 2.

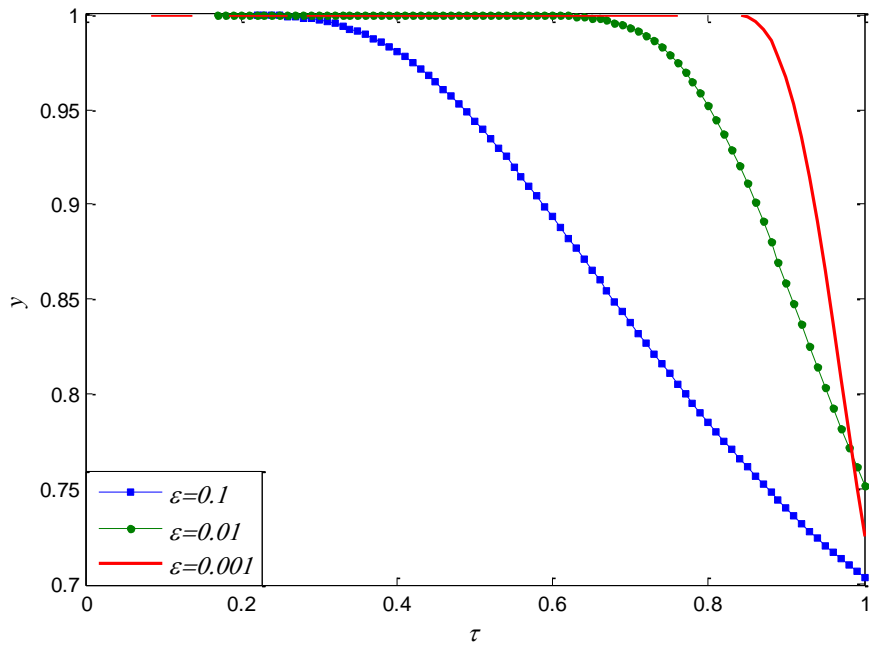


Figure 8: Behavior of $y(\xi, \tau)$ for different values of $\bar{\epsilon}$.

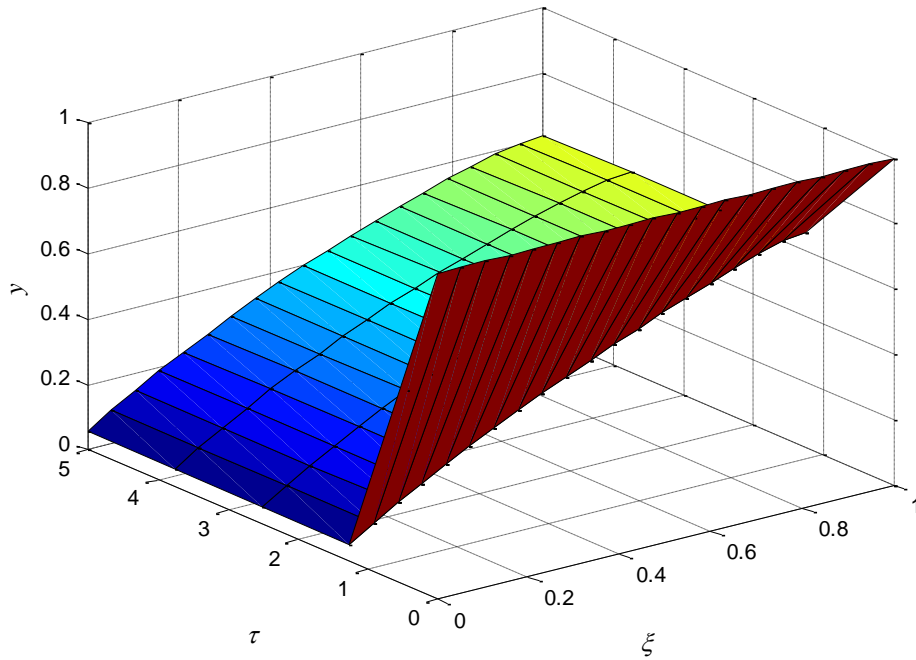


Figure 9a: 3D behaviour of $y(\xi, \tau)$ for $\bar{\epsilon} = 2^{-4}$.

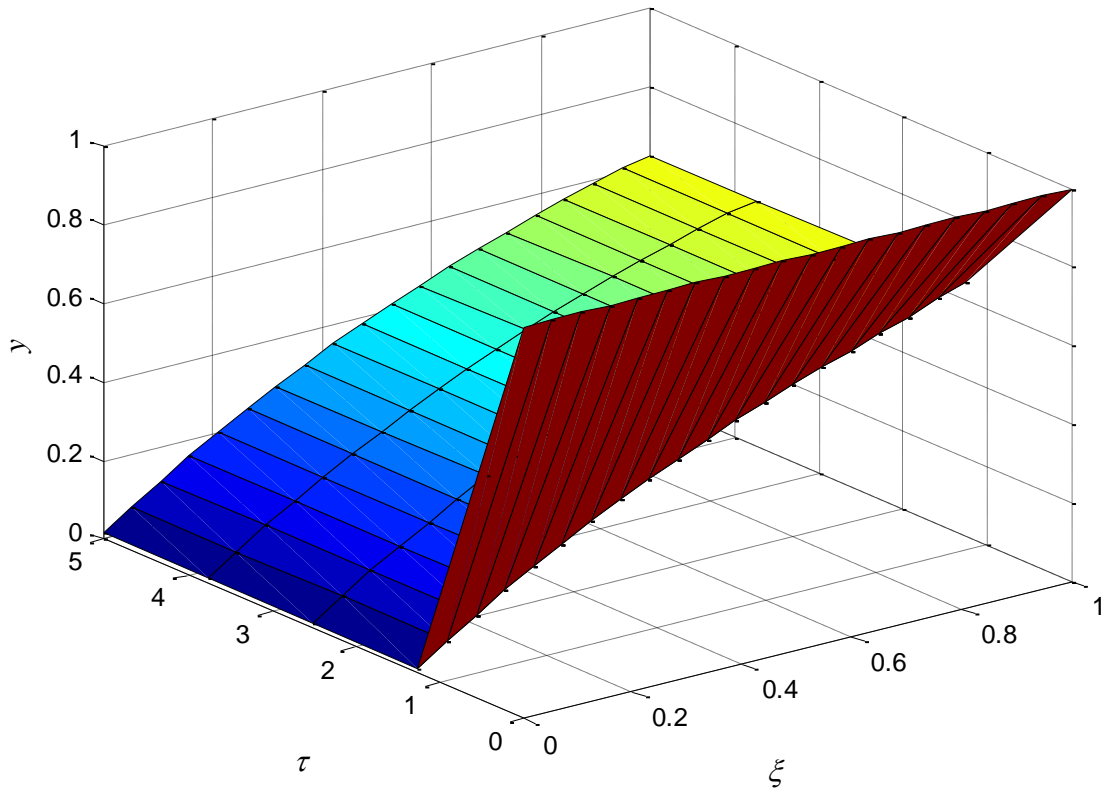


Figure 9b: 3D behaviour of $y(\xi, \tau)$ for $\bar{\epsilon} = 2^{-6}$.

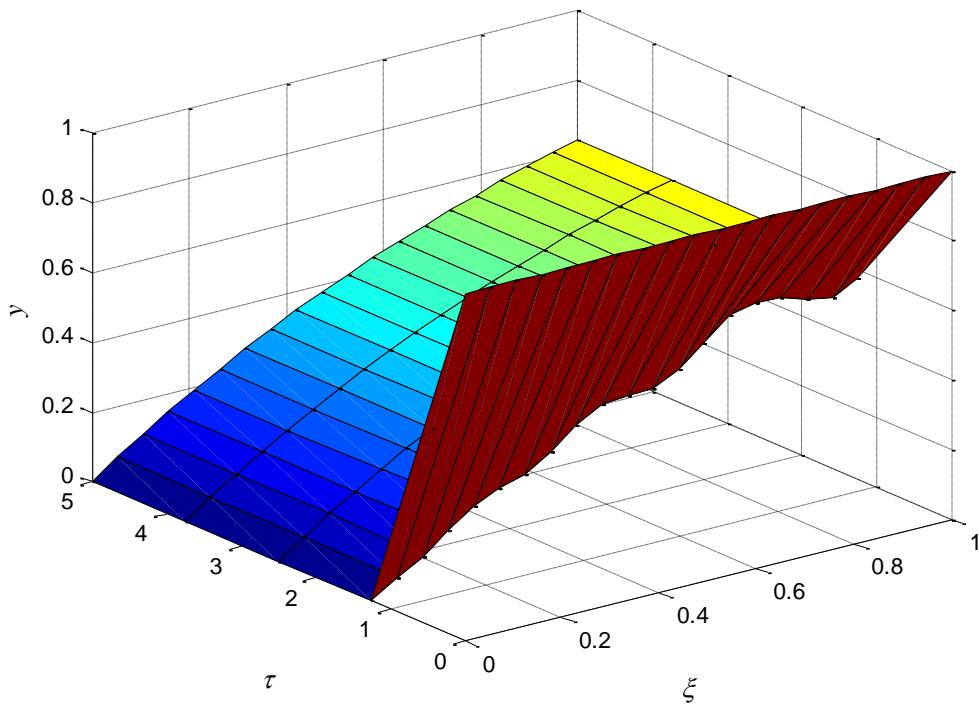


Figure 9c: 3D behaviour of $y(\xi, \tau)$ for $\bar{\epsilon} = 2^{-10}$.

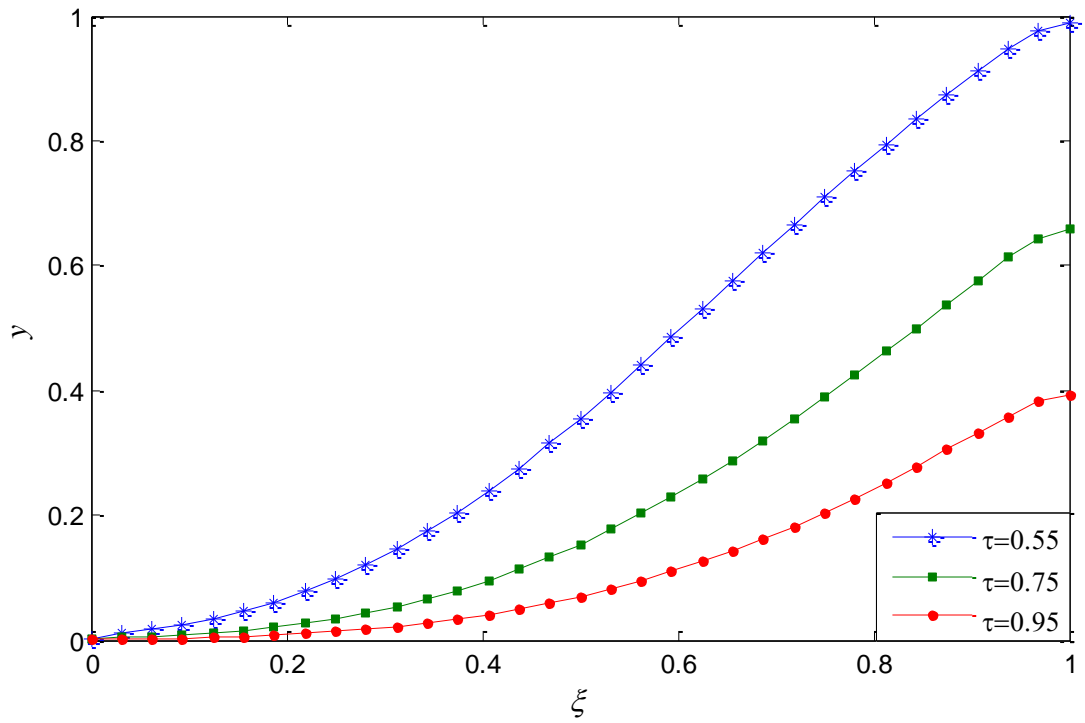


Figure 10: Behavior of $y(\xi, \tau)$ for $\bar{\varepsilon} = 2^{-4}$ at different time intervals for Problem 3.

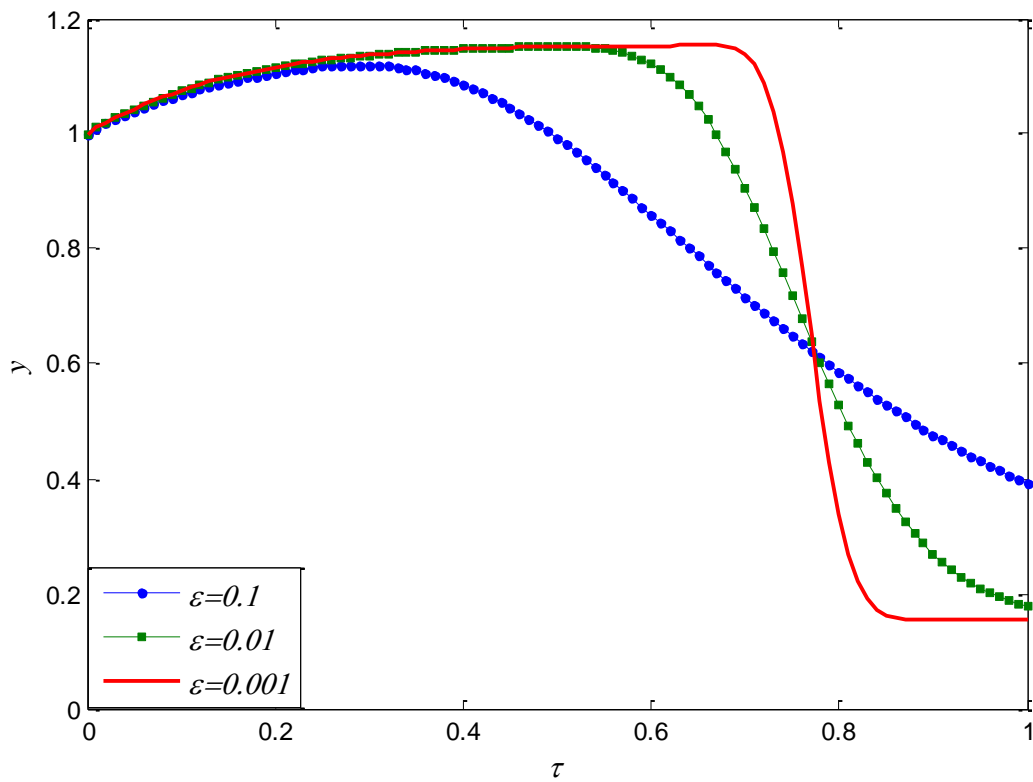


Figure 11: Behavior of $y(\xi, \tau)$ for different values of $\bar{\varepsilon}$.

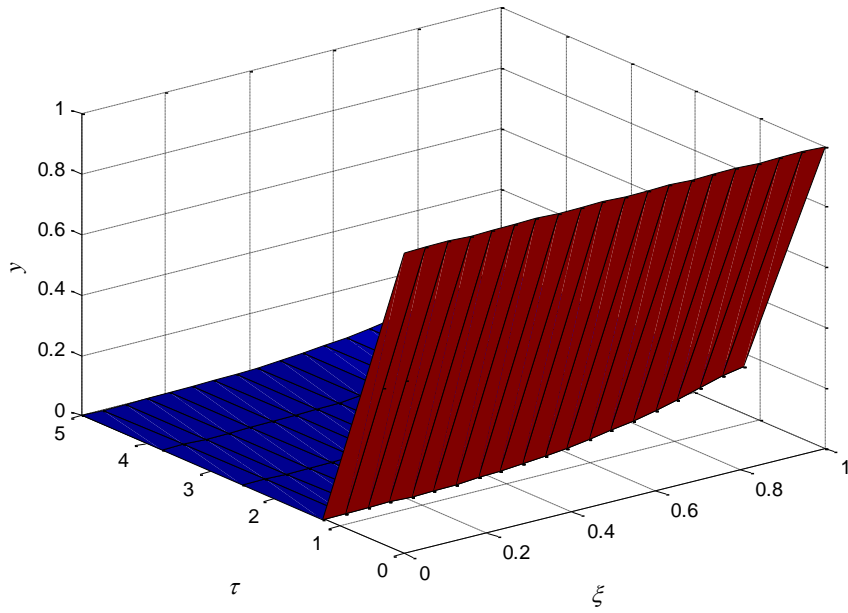


Figure 12a: 3D behaviour of $y(\xi, \tau)$ for $\bar{\varepsilon} = 2^{-4}$.

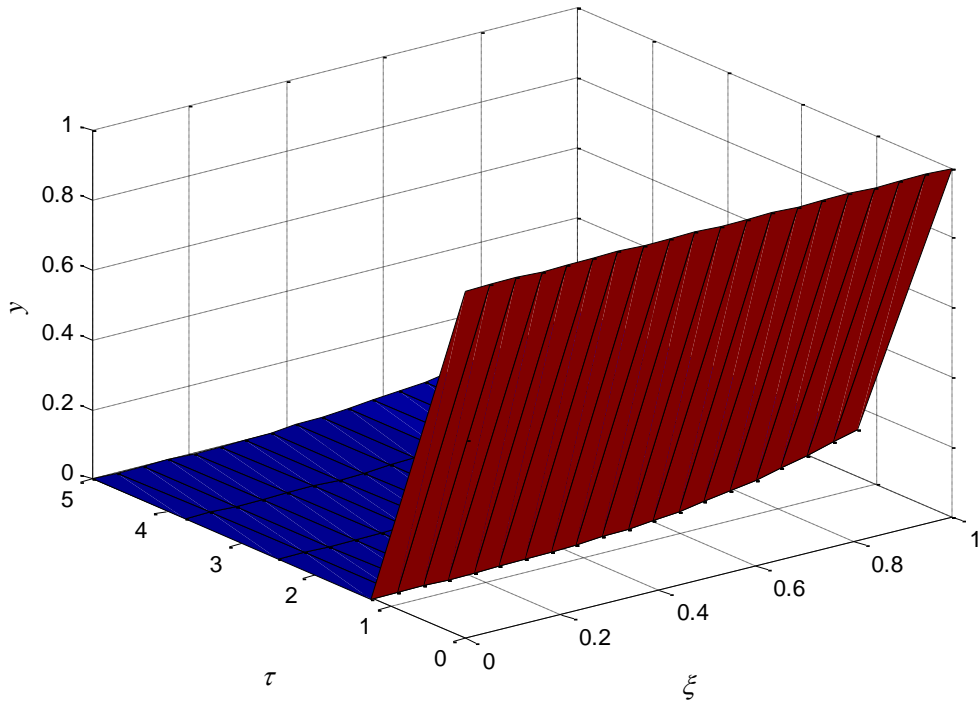


Figure 12b: 3D behaviour of $y(\xi, \tau)$ for $\bar{\varepsilon} = 2^{-6}$.

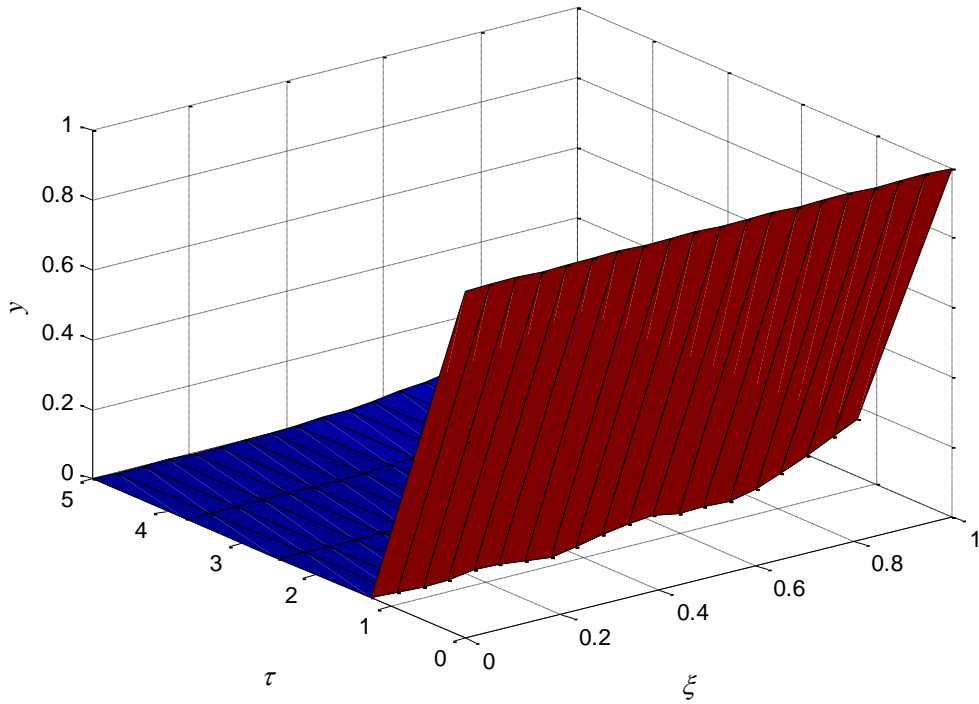


Figure 12c: 3D behaviour of $y(\xi, \tau)$ for $\bar{\varepsilon} = 2^{-10}$.

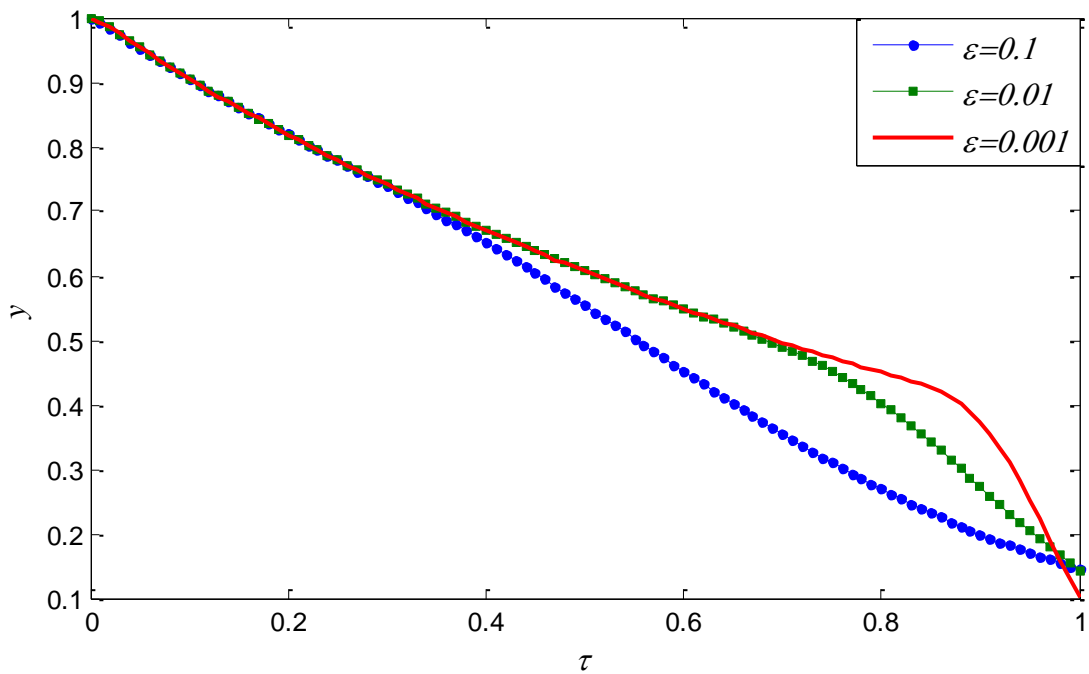


Figure 13: Behavior of $y(\xi, \tau)$ for different values of $\bar{\varepsilon}$ for Problem 4.

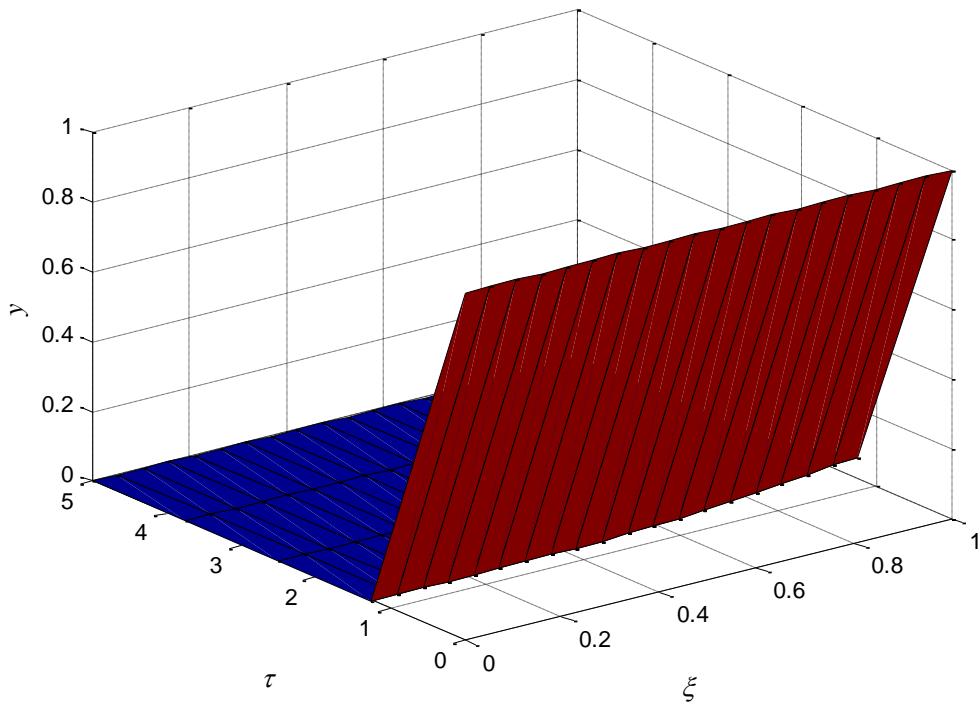


Figure 14a: 3D behaviour of $y(\xi, \tau)$ for $\bar{\varepsilon} = 2^{-4}$.

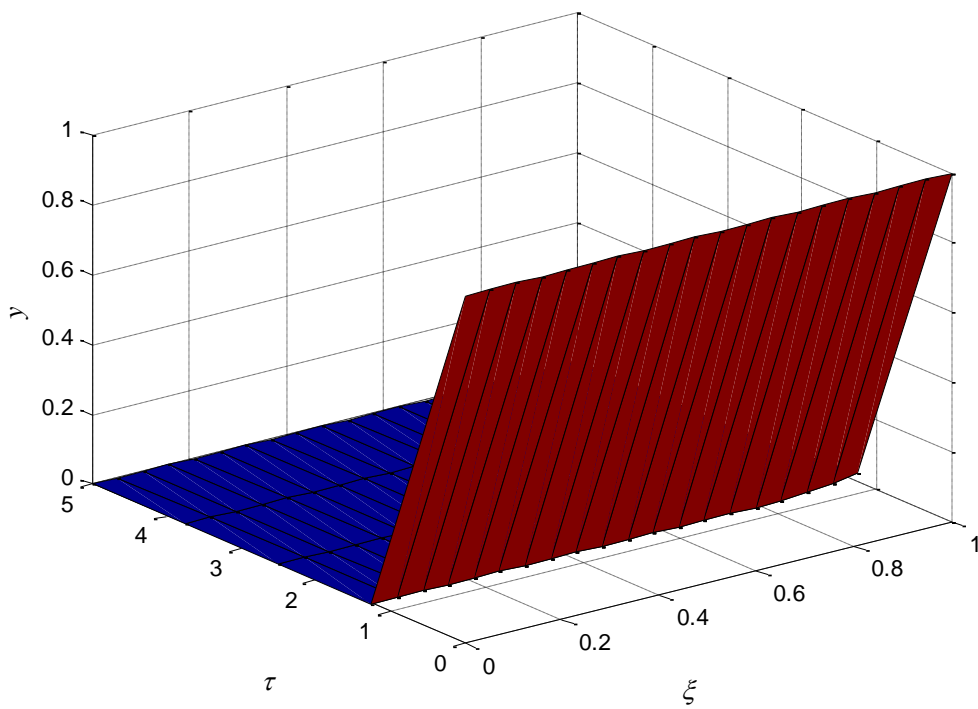


Figure 14b: 3D behaviour of $y(\xi, \tau)$ for $\bar{\varepsilon} = 2^{-6}$.

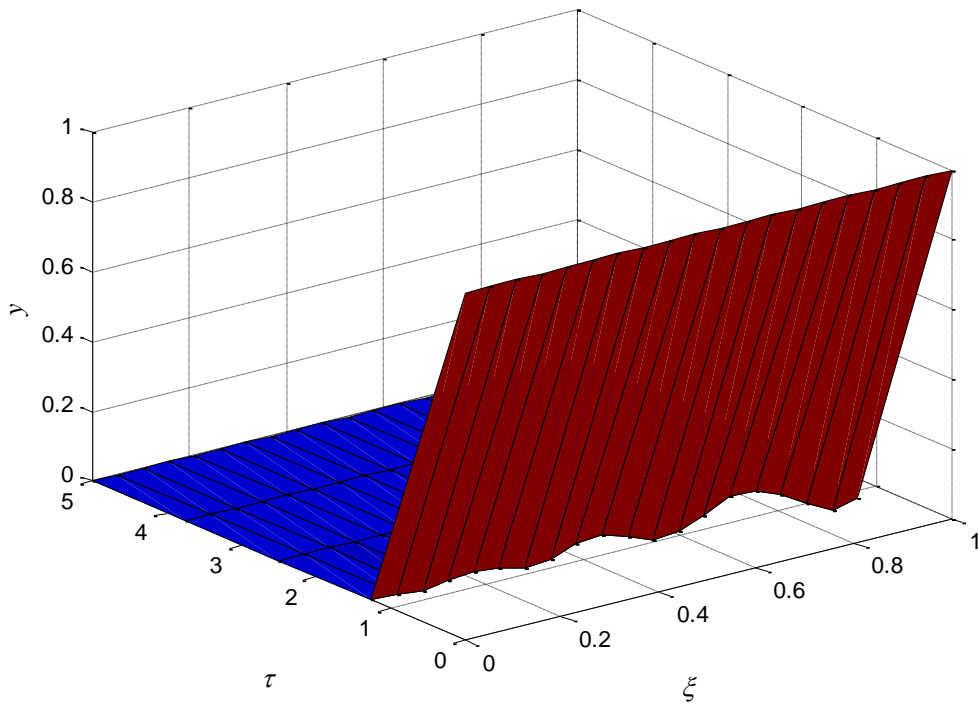


Figure 14c: 3D behaviour of $y(\xi, \tau)$ for $\bar{\varepsilon} = 2^{-10}$.

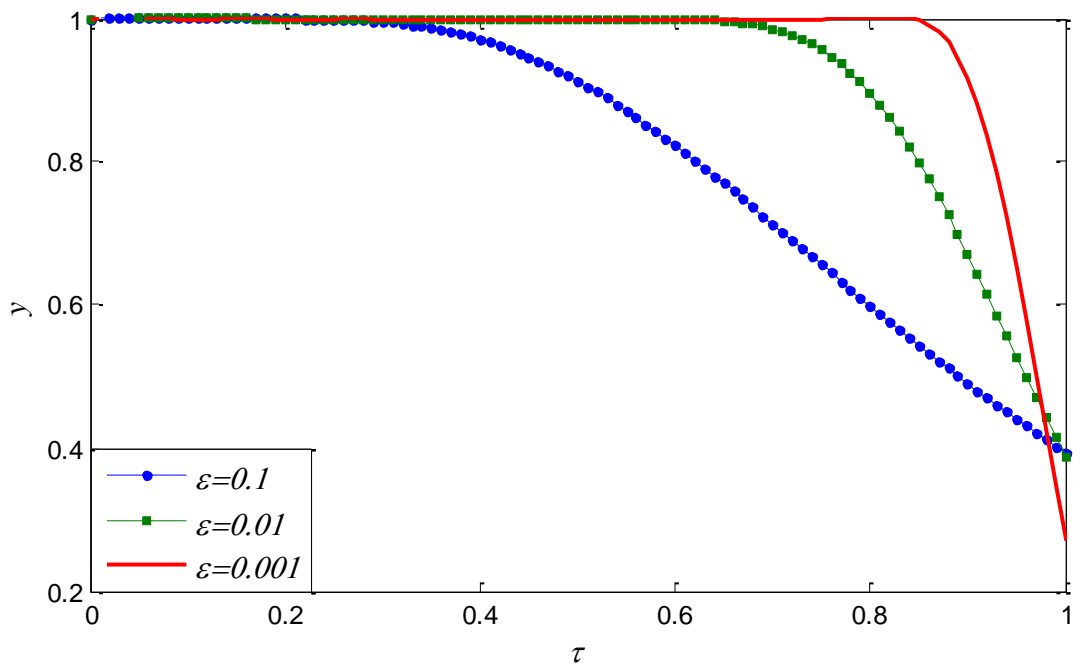


Figure 15: Behavior of $y(\xi, \tau)$ for different values of $\bar{\varepsilon}$ for Problem 5.

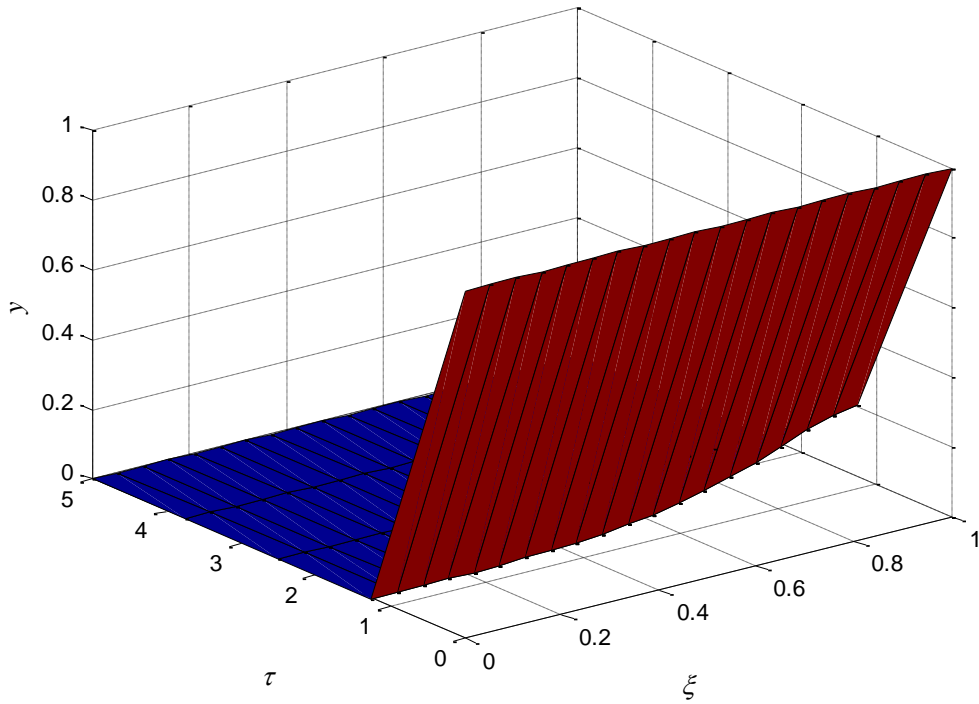


Figure 16a: 3D behaviour of $y(\xi, \tau)$ for $\bar{\varepsilon} = 2^{-4}$.

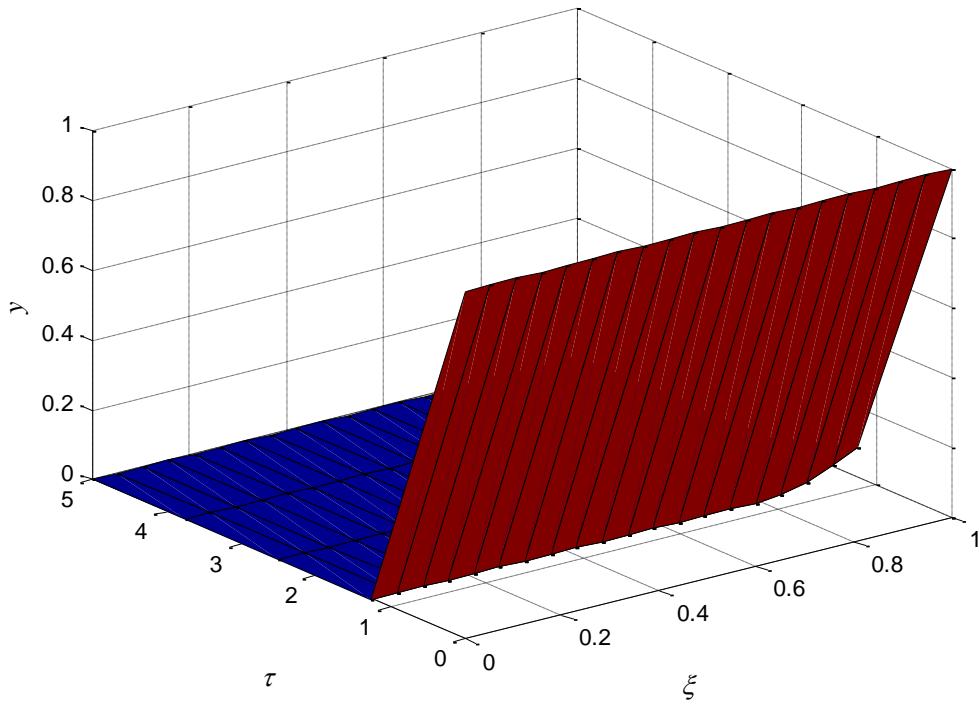


Figure 16b: 3D behaviour of $y(\xi, \tau)$ for $\bar{\varepsilon} = 2^{-6}$.

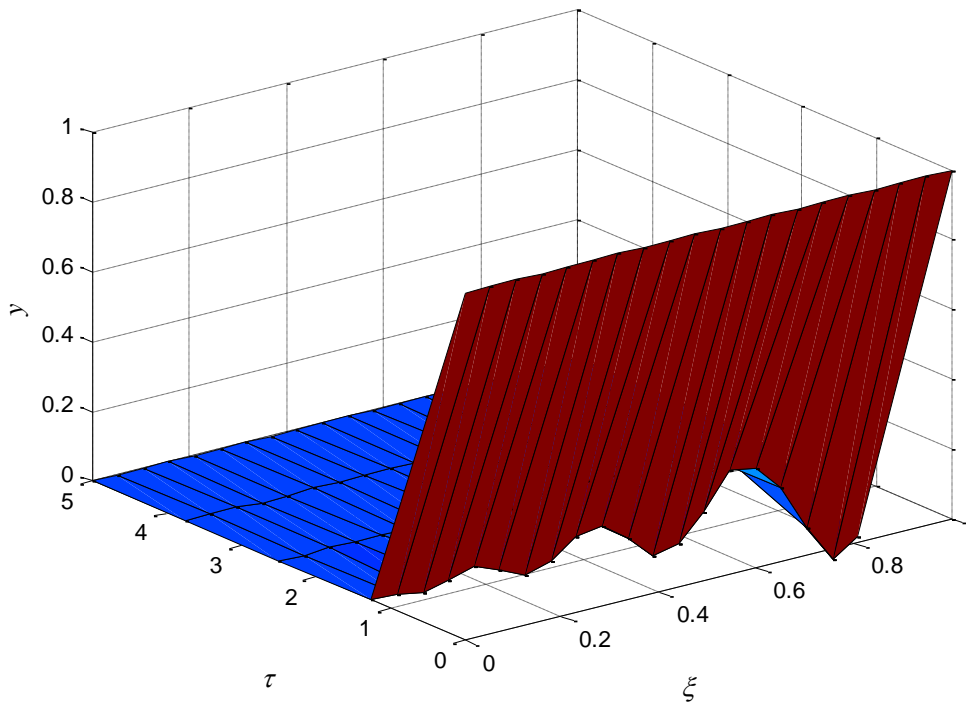


Figure 16c: 3D behaviour of $y(\xi, \tau)$ for $\bar{\varepsilon} = 2^{-10}$.

Table 1- $\bar{\varepsilon}$ -uniform error analysis for Problem 1.

$\bar{\varepsilon}$	$E_{\bar{\varepsilon}}^m$				
	$m = 8$	$m = 16$	$m = 32$	$m = 64$	$m = 128$
2^0	1.6900×10^{-3}	4.0800×10^{-4}	1.0020×10^{-4}	2.4800×10^{-5}	6.1000×10^{-6}
2^{-2}	2.4920×10^{-2}	1.2597×10^{-2}	6.3530×10^{-3}	3.1940×10^{-3}	1.6018×10^{-3}
2^{-4}	1.3042×10^{-2}	4.2572×10^{-3}	1.8113×10^{-3}	8.6330×10^{-4}	4.2660×10^{-4}
2^{-6}	3.0938×10^{-3}	1.3550×10^{-4}	8.1000×10^{-6}	2.0000×10^{-7}	1.0000×10^{-7}
2^{-8}	2.3303×10^{-3}	3.6600×10^{-4}	3.7600×10^{-5}	2.1000×10^{-6}	1.0000×10^{-7}
2^{-10}	1.3851×10^{-3}	3.9390×10^{-4}	9.5600×10^{-5}	9.3000×10^{-6}	3.0000×10^{-7}
2^{-12}	1.1296×10^{-3}	3.5750×10^{-4}	1.1560×10^{-4}	2.4900×10^{-5}	1.9000×10^{-6}
2^{-14}	1.0665×10^{-3}	3.4640×10^{-4}	1.0930×10^{-4}	3.5100×10^{-5}	5.9000×10^{-6}
2^{-16}	1.0508×10^{-3}	3.4380×10^{-4}	1.0580×10^{-4}	3.5900×10^{-5}	9.9000×10^{-6}
2^{-18}	1.0470×10^{-3}	3.4310×10^{-4}	1.0480×10^{-4}	3.5300×10^{-5}	1.5100×10^{-5}
2^{-20}	1.0460×10^{-3}	3.4300×10^{-4}	1.0450×10^{-4}	3.5100×10^{-5}	1.1800×10^{-5}
E^m	2.4920×10^{-2}	1.2597×10^{-2}	6.3530×10^{-3}	3.1940×10^{-3}	1.6018×10^{-3}
p^m	9.8422×10^{-1}	9.8757×10^{-1}	9.9207×10^{-1}	9.9567×10^{-1}	

Table 2- $\bar{\varepsilon}$ -uniform error analysis for Problem 2.

$\bar{\varepsilon}$	$E_{\bar{\varepsilon}}^m$				
	$m = 8$	$m = 16$	$m = 32$	$m = 64$	$m = 128$
2^0	1.4702×10^{-3}	3.5300×10^{-4}	8.6800×10^{-5}	2.1600×10^{-5}	5.3000×10^{-6}
2^{-2}	2.5127×10^{-2}	1.2837×10^{-2}	6.4884×10^{-3}	3.2627×10^{-3}	1.6360×10^{-3}
2^{-4}	2.2729×10^{-2}	8.1878×10^{-3}	3.6369×10^{-3}	1.7576×10^{-3}	8.7150×10^{-4}

2^{-6}	1.2406×10^{-3}	9.5400×10^{-5}	2.9600×10^{-5}	1.0800×10^{-5}	4.7000×10^{-6}
2^{-8}	3.7452×10^{-3}	6.8500×10^{-5}	2.6000×10^{-6}	1.0000×10^{-7}	0.0000×10^0
2^{-10}	3.3890×10^{-3}	5.1600×10^{-5}	8.8000×10^{-6}	7.0000×10^{-7}	1.0000×10^{-7}
2^{-12}	3.1610×10^{-3}	8.2000×10^{-5}	2.1500×10^{-5}	4.1000×10^{-6}	3.0000×10^{-7}
2^{-14}	3.0930×10^{-3}	8.1000×10^{-5}	4.2900×10^{-5}	5.4000×10^{-6}	1.2000×10^{-6}
2^{-16}	3.0760×10^{-3}	7.9000×10^{-5}	5.0100×10^{-5}	6.5000×10^{-6}	7.0000×10^{-7}
2^{-18}	3.0700×10^{-3}	7.9000×10^{-5}	5.2500×10^{-5}	7.0000×10^{-6}	4.0000×10^{-7}
2^{-20}	3.0700×10^{-3}	7.9000×10^{-5}	5.2700×10^{-5}	7.3000×10^{-6}	3.0000×10^{-7}
E^m	2.5127×10^{-2}	1.2837×10^{-2}	6.4884×10^{-3}	3.2627×10^{-3}	1.6360×10^{-3}
p^m	9.6893×10^{-1}	9.8437×10^{-1}	9.9180×10^{-1}	9.9589×10^{-1}	

Table 3- $\bar{\epsilon}$ -uniform error analysis for Problem 3.

$\bar{\epsilon}$	$E_{\bar{\epsilon}}^n$				
	$m = 16$	$m = 32$	$m = 64$	$m = 128$	$m = 256$
2^0	5.6770×10^{-4}	1.3730×10^{-4}	2.9800×10^{-5}	1.0000×10^{-5}	4.4000×10^{-6}
2^{-2}	2.5147×10^{-2}	1.2644×10^{-2}	6.3450×10^{-3}	3.1800×10^{-3}	1.5866×10^{-3}
2^{-4}	2.0353×10^{-2}	8.8430×10^{-3}	4.2300×10^{-3}	2.1000×10^{-3}	1.0490×10^{-3}
2^{-6}	6.1600×10^{-4}	1.7600×10^{-4}	5.7000×10^{-5}	0.0000×10^0	4.4000×10^{-5}
2^{-8}	3.7000×10^{-5}	1.3000×10^{-5}	2.2000×10^{-5}	0.0000×10^0	2.1000×10^{-5}
2^{-10}	4.2800×10^{-4}	5.0000×10^{-5}	5.0000×10^{-6}	0.0000×10^0	1.0000×10^{-6}
2^{-12}	9.8500×10^{-4}	2.3000×10^{-4}	1.4000×10^{-5}	0.0000×10^0	2.1000×10^{-5}
2^{-14}	1.2160×10^{-3}	2.1800×10^{-4}	1.4500×10^{-4}	0.0000×10^0	2.6000×10^{-5}
2^{-16}	1.2830×10^{-3}	1.7800×10^{-4}	2.2300×10^{-4}	0.0000×10^0	2.7000×10^{-5}
2^{-18}	1.3010×10^{-3}	1.6300×10^{-4}	1.4800×10^{-4}	1.0000×10^{-4}	2.8000×10^{-5}
2^{-20}	1.3050×10^{-3}	1.5900×10^{-4}	1.5400×10^{-4}	1.0000×10^{-4}	2.9000×10^{-5}
E^m	2.5147×10^{-2}	1.2644×10^{-2}	6.3450×10^{-3}	3.1800×10^{-3}	1.5866×10^{-3}
p^m	9.9193×10^{-1}	9.9476×10^{-1}	9.9659×10^{-1}	1.0031×10^0	

Table 4- $\bar{\epsilon}$ -uniform error analysis for Problem 4.

$\bar{\epsilon}$	$E_{\bar{\epsilon}}^m$				
	$m = 8$	$m = 16$	$m = 32$	$m = 64$	$m = 128$
2^0	1.4716×10^{-3}	3.5440×10^{-4}	8.6900×10^{-5}	2.1500×10^{-5}	5.4000×10^{-6}
2^{-2}	2.5112×10^{-2}	1.2836×10^{-2}	6.4884×10^{-3}	3.2626×10^{-3}	1.6361×10^{-3}
2^{-4}	2.2741×10^{-2}	8.1864×10^{-3}	3.6368×10^{-3}	1.7576×10^{-3}	8.7140×10^{-4}
2^{-6}	1.2381×10^{-3}	9.5700×10^{-5}	2.9600×10^{-5}	1.0800×10^{-5}	4.7000×10^{-6}
2^{-8}	3.8221×10^{-3}	6.8600×10^{-5}	2.7000×10^{-6}	0.0000×10^0	1.0000×10^{-7}
2^{-10}	3.4640×10^{-3}	5.1900×10^{-5}	8.8000×10^{-6}	7.0000×10^{-7}	0.0000×10^0
2^{-12}	3.2323×10^{-3}	8.3100×10^{-5}	2.1200×10^{-5}	4.1000×10^{-6}	3.0000×10^{-7}
2^{-14}	3.1640×10^{-3}	8.1600×10^{-5}	4.2500×10^{-5}	5.3000×10^{-6}	1.3000×10^{-6}
2^{-16}	3.1463×10^{-3}	8.0000×10^{-5}	5.0000×10^{-5}	6.6000×10^{-6}	6.0000×10^{-7}
2^{-18}	3.1419×10^{-3}	7.9400×10^{-5}	5.2100×10^{-5}	7.1000×10^{-6}	4.0000×10^{-7}
2^{-20}	3.1407×10^{-3}	7.9300×10^{-5}	5.2600×10^{-5}	7.3000×10^{-6}	3.0000×10^{-7}
E^m	2.5112×10^{-2}	1.2836×10^{-2}	6.4884×10^{-3}	3.2626×10^{-3}	1.6361×10^{-3}
p^m	9.6819×10^{-1}	9.8423×10^{-1}	9.9184×10^{-1}	9.9576×10^{-1}	

Table 5- $\bar{\epsilon}$ -uniform error analysis for Problem 5.

$\bar{\epsilon}$	$E_{\bar{\epsilon}}^m$				
	$m = 8$	$m = 16$	$m = 32$	$m = 64$	$m = 128$
2^0	2.6208×10^{-3}	6.3130×10^{-4}	1.5470×10^{-4}	3.8300×10^{-5}	9.5000×10^{-6}
2^{-2}	3.8539×10^{-2}	1.9464×10^{-2}	9.8153×10^{-3}	4.9345×10^{-3}	2.4748×10^{-3}
2^{-4}	2.0994×10^{-2}	6.6237×10^{-3}	2.8012×10^{-3}	1.3339×10^{-3}	6.5900×10^{-4}
2^{-6}	2.0436×10^{-3}	4.8600×10^{-5}	1.3000×10^{-6}	5.0000×10^{-7}	3.0000×10^{-7}
2^{-8}	1.4490×10^{-4}	1.5690×10^{-4}	7.6000×10^{-6}	1.0000×10^{-7}	0
2^{-10}	1.7878×10^{-3}	3.3700×10^{-4}	3.4100×10^{-5}	1.8000×10^{-6}	1.0000×10^{-7}
2^{-12}	2.2090×10^{-3}	4.2570×10^{-4}	5.8000×10^{-5}	6.7000×10^{-6}	7.0000×10^{-7}
2^{-14}	2.3114×10^{-3}	4.4590×10^{-4}	7.5400×10^{-5}	4.7000×10^{-6}	1.8000×10^{-6}
2^{-16}	2.3367×10^{-3}	4.5030×10^{-4}	8.1500×10^{-5}	5.6000×10^{-6}	8.0000×10^{-7}
2^{-18}	2.3430×10^{-3}	4.5130×10^{-4}	8.3200×10^{-5}	6.1000×10^{-6}	1.9000×10^{-6}
2^{-20}	2.3445×10^{-3}	4.5170×10^{-4}	8.3600×10^{-5}	7.0000×10^{-6}	3.0000×10^{-6}
E^m	3.8539×10^{-2}	1.9464×10^{-2}	9.8153×10^{-3}	4.9345×10^{-3}	2.4748×10^{-3}
p^m	9.8551×10^{-1}	9.8770×10^{-1}	9.9213×10^{-1}	9.9559×10^{-1}	

Conclusion

A numerical scheme based on CHCM has been presented for the solution of Initial value problem. Numerical results demonstrate the stability and accuracy of the method for any value of $\bar{\epsilon}$. From these figures and tables, it is observed that the accuracy of the method is of order (h^4). This method is easy to implement and yields very accurate results.

References

[1]. Grahs L.E. (1974). Washing of cellulose fibres, Analysis of displacement washing operation, Ph.D. Thesis, Chalmers University of Technology, Goteborg, Sweden.

[2]. Al-Jabari M., VanHeiningen A.R.P. & Van De Ven T.G.M. (1994). Modeling the flow and the deposition of fillers in packed bed of pulp fibers. Journal of Pulp and Paper Science; 20(9), J249-J253.

[3]. Maleknejad K., Aghazadeh N. & Mollapourasl R. (2006). Numerical solution of Fredholm integral equation of the first kind with collocation method and estimation of error bound. Applied Mathematics and Computation; 179, 352–359.

[4]. Shen Y. & Lin W. (2006). Collocation method for the natural boundary integral equation. Applied Mathematics Letters; 19(11), 1278–1285.

[5]. Soliman M.A. & Alhumaizi K.I (2004). Studies on the Method of Orthogonal Collocation VI: A Moving Collocation Method for the Solution of the Transient Heat Conduction Problem. Journal of King Saud University Engineering Science; 17, 213-226.

[6]. Carey G.F. & Finlayson B.A. (1975). Orthogonal collocation on finite elements. Chemical Engineering Science; 30, 587-596.

[7]. Arora S., Dhaliwal S. S. & Kukreja V.K. (2006b). Simulation of washing of packed bed of porous particles by orthogonal collocation on finite element. Computers and Chemical Engineering; 30, 1054-1060.

[8]. Islam S. U., Aziz I. & Sarler B. (2010). The numerical solution of second-order boundary-value problems by collocation method with the Haar wavelets. Mathematical and Computer Modelling; 52, 1577-1590.

[9]. Kim S. D. & Shin B. C. (2002). Preconditioning C^1 Lagrange polynomial spline collocation method of elliptic equations by finite element method. Applied Mathematics and Computation; 132(2-3), 599-61.

[10]. Gracia J. L. & Riordan E. O. (2012) A singularly perturbed parabolic problem with a layer in the initial condition. Applied Mathematics and Computation; 219(21), 498–510.

[11]. Luo Z., Li H. & Sun P. (2013). A reduced-order Crank–Nicolson finite volume element formulation based on POD method for parabolic equations. Applied Mathematics and Computation; 219, 5887–900.

-
- [12]. Arora S., Dhaliwal S. S. & Kukreja V.K. (2005). Solution of two point boundary value problems using orthogonal collocation on finite elements. *Applied Mathematics and Computation*; 171, 358-370.
- [13]. Yang Y., Chen Y. & Huang Y. (2014). Convergence analysis of the Jacobi spectral-collocation method for fractional integro-differential equations. *Acta Mathematica Scientia*; 34(3), 673-690.
- [14]. Fernandes R. I., Bialecki B. & Fairweather G. (2015). An ADI extrapolated Crank–Nicolson orthogonal spline collocation method for nonlinear reaction–diffusion systems on evolving domains. *Journal of Computational Physics*; 299, 561-580.
- [15]. Nadukandi P., Onate E. & Garcia J. (2012). A high resolution Petrov-Galerkin method for the 1D convection-diffusion reaction problem. Part II—A multidimensional extension. *Computer Methods in Applied Mechanics and Engineering*; (213–16), 327-352.
- [16]. Wei L., He Y., Zhang X. & Wang S. (2012). Analysis of an implicit fully discrete local discontinuous Galerkin method for the time-fractional Schrodinger equation. *Finite Elements in Analysis and Design*; 59, 28-34.
- [17]. Parvazinia M. (2012). An elemental scale adjustment method for the finite element and finite difference solutions of diffusion-reaction and convection–diffusion equations. *Finite Elements in Analysis and Design*; 58, 1-9.
- [18]. Villadsen J. & Stewart W.E. (1967). Solution of boundary value problems by orthogonal collocation. *Chemical Engineering Science*; 22, 1483-1501.
- [19]. Dyksen W. R. & Lynch R. E. (2000). A new decoupling technique for the Hermite cubic collocation equations arising from boundary value problems. *Mathematics and Computers in Simulation*; 54, 359–372.
- [20]. Brill S. H. (2002). Analytic solution of Hermite collocation discretization of the steady state convection-diffusion equation. *International Journal of Differential Equations and Application*; 4, 141-155.
- [21]. Swartz B. K. and Varge R. S. (1972). Error bounds for spline and L -spline interpolation. *Journal of Approximation Theory*; 6, 6-49.
- [22]. Kumar D. & Kadalbajoo M. K. (2011). A parameter-uniform numerical method for time-dependent singularly perturbed differential–difference equations. *Application of Mathematical Modelling*; 35, 2805–19.
- [23]. Farrell P. A. & Hagarty H. (1991). On the determination of the order of uniform convergence. *Proceeding of 13th IMACS world congress, Dublin, Ireland*, 501-502.